Dalton Transactions

ROYAL SOCIETY OF CHEMISTRY

PAPER

View Article Online
View Journal

Cite this: DOI: 10.1039/d5dt00977d

Luminescent ionic heterobimetallic diphosphine-β-diketiminate complexes

Steven Kebernik,[a] Frederic Krätschmer,[a] Xiaofei Sun [a] and Peter W. Roesky *[a,b]

The syntheses of luminescent heterobimetallic ionic complexes based on the bis(phosphine)-functionalized β-diketiminate ligand $[HC\{(CH_3)C\}_2\{(o\text{-}[P(C_6H_5)_2]_2C_6H_4)N\}_2]^-$ (PNac) are reported. This orthogonal ligand is characterized by its PNNP pocket, which contains both hard and soft donor sites and therefore enables the selective coordination of two different metal ions in spatial proximity, significantly changing the photoluminescent properties. Salt elimination reaction of [PNacK] with zinc chloride yields the monometallic complex [PNacZnCl], in which the zinc ion is square-pyramidally coordinated within the PNNP pocket. The introduction of the coinage metal ions Au^I, Ag^I and Cu^I into the PNNP pocket as a second metal ion is achieved by simple complexation reactions using their corresponding weakly coordinating anion (WCA) salts. In the resulting ionic heterobimetallic complexes $[PNacZnCl(thf)M]^+$ (M = Au, Ag, and Cu), the coinage metal ions are linearly coordinated by the two phosphine units, while the zinc ion is tetrahedrally coordinated at the diketiminate unit. The photoluminescent properties are significantly altered by the spatial proximity of the two metal ions. Furthermore, the ionic gold–copper complex $[PNacAuCu(MeCN)]^+$ was isolated by introducing Cu^I into the monometallic gold complex using the same method.

Received 25th April 2025,
Accepted 27th July 2025

DOI: 10.1039/d5dt00977d

rsc.li/dalton

Introduction

In homo- or heterobimetallic systems, the presence of two metal centers can result in unique luminescent properties that may not be achievable in monometallic compounds, as a result of cooperative effects.[1–6] In addition to influencing photophysical properties, this cooperativity is also of great interest for improving catalytic properties or increasing chemical reactivity.[7–13] One of the best-known examples of cooperativity in catalysis is probably the multimetallic catalysts developed by Peris *et al.*, based on triazolyldiylidene complexes with Ir, Pd and/or Rh metal centers.[8,14–19] In addition, it is known that complexes with metallophilic contacts often exhibit rich photophysical properties. These metallophilic contacts are influenced by the multimetallic scaffold, making cooperative effects important in adjusting the luminescence properties of multimetallic systems.[20–23] In monometallic complexes containing elements with high atomic numbers, such as gold, the enhanced spin–orbit coupling (heavy metal effect) allows efficient intersystem crossing (ISC) from excited singlet to lower lying triplet states, resulting in phosphorescence from these triplet states to the ground singlet state, typically with emission decay times in the microsecond range.[20] In general, cooperativity within bimetallic systems can be categorized into four types (Fig. 1): systems with direct contacts of metal–metal bonds (**A**), systems with metallophilic interactions (**B**), complexes in which the metal atoms are spatially separated by a linker, (**C**) and those in which metals are brought into close proximity by a rigid ligand (**D**).[6,24–32]

The fact that the photoluminescence properties of multimetallic complexes can be tuned by structural changes, such as metal-to-metal distances and the combination of metals involved, offers potential for applications in areas such as OLED design and sensor technology.[33,34] In order to specifically coordinate two different metal ions within the same ligand framework, so-called orthogonal ligand systems must be designed and synthesized.[35] For the development of such bifunctional ligands, Pearson's principle of hard and soft acids and bases (HSAB) can be applied.[36–38] In particular, coinage metals are known for their different behavior towards hard and soft coordination sites.[30,31,39–41] As the "softest" cation, gold(I) prefers "soft" donors, while copper(I) as a "hard" metal ion exhibits a strong affinity for "hard" donors; silver(I) can coordinate to both "hard" and "soft" donors.[35] Together with the structural design of the ligand systems in terms of steric demands and spatial proximity of the donor sites, specific arrangements of metal ions as well as direct metal···metal interactions can be enforced.[42] A suitable system for the preparation of heterobimetallic systems is the bis(diphenyl)phosphine-functionalized β-diketiminato ligand system $[HC\{(CH_3)C\}_2\{(o\text{-}[P(C_6H_5)_2]_2C_6H_4)N\}_2]^-$ (PNac), which

[a]Institute of Inorganic Chemistry, Karlsruhe Institute of Technology, Engesserstr. 15, 76131 Karlsruhe, Germany. E-mail: roesky@kit.edu
[b]Institute of Nanotechnology, Karlsruhe Institute of Technology, Kaiserstr. 12, 76131 Karlsruhe, Germany

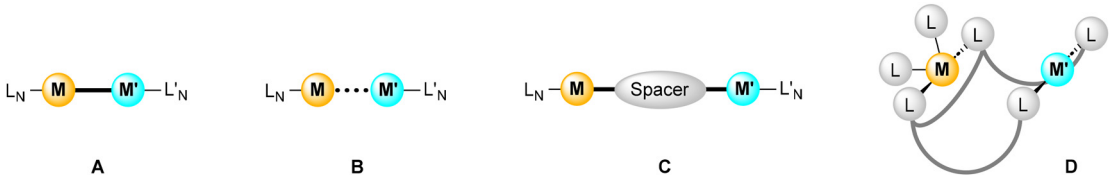

Fig. 1 Bimetallic systems: (A) with metal–metal bond interaction, (B) metallophilic interaction, (C) bridged bimetallic compounds, and (D) spatial proximity of metal centers driven by rigid ligands.[32]

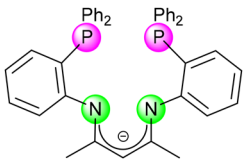

Fig. 2 Monoanionic PNac as an orthogonal ligand with hard nitrogen (green) and soft phosphorous (pink) donor sites.[32,43–45]

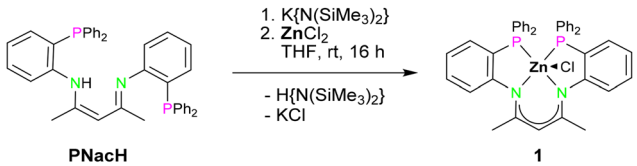

Scheme 1 Synthesis of the monometallic compound [PNacZnCl] (**1**).

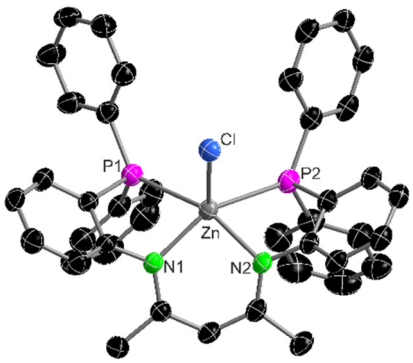

Fig. 3 Molecular structure of [PNacZnCl] (**1**) in the solid state with ellipsoids drawn at 50% probability. Hydrogen atoms and non-coordinating THF molecules are omitted for clarity. Selected distances [Å] and angles [°]: Zn–Cl 2.2106(12), Zn–P1 2.6053(13), Zn–P2 2.6029(14), Zn–N1 2.038 (4), Zn–N2 2.046(3); P1–Zn–P2 105.84(4), N1–Zn–N2 90.32(14), N1–Zn–P1 74.64(10), and N2–Zn–P2 73.63(11).

contains two "soft" phosphine donor sites and a "hard" β-diketiminato donor site (Fig. 2). With this monoanionic ligand, a wide range of monometallic compounds of various transition metals and group 14 elements with different coordination modes as well as the neutral heterobimetallic group 11/12 compounds has been recently reported.[32,43–47]

It is well known that in the condensed phase, packing effects or interactions with counterions and solvent molecules can have a considerable influence on the PL properties.[48–55] Herein, we present a synthetic protocol for ionic heterobimetallic complexes of the PNac ligand with zinc and coinage metals. The PL properties of these heterobimetallic compounds were investigated in the solid state, in solution at low temperature (77 K) and at ambient temperature. Compared to the bimetallic neutral PNac complexes [PNacMZnCl$_2$] (M = Ag, Au),[32,47] we were interested in assessing how the altered coordination environment around Zn influences the PL properties. Furthermore, the ionic nature of these compounds could potentially allow PL studies to be carried out in the gas phase.

Results and discussion

The monometallic compound [PNacZnCl] (**1**) was synthesized by *in situ* deprotonation of the proligand PNacH by using potassium bis(trimethylsilyl)amide, followed by subsequent salt-elimination reaction with zinc chloride (Scheme 1). Crystals of **1** suitable for single-crystal X-ray diffraction analysis were obtained by layering the tetrahydrofuran (THF) solution with *n*-pentane.

In compound **1**, the zinc ion is located within the PNNP pocket of the PNac ligand and adopts a square-pyramidal coordination due to an additional chloride ion (Fig. 3). This coordination geometry is comparable to that of other transition metal complexes of the PNac ligand (Fe^{II}, Co^{II}, Ni^{II}) with a coordinating chloride anion.[43,46] In the $^{31}P\{^1H\}$ NMR spectrum of compound **1**, one singlet resonance was detected at δ = −26.6 ppm, which is slightly high-field shifted compared to the proligand (δ = −14.5 ppm).[43]

To obtain the target ionic bimetallic complexes of the general formula [PNacZnCl(thf)M][WCA] (**2**: Au, **3**: Ag, **4**: Cu; WCA = weakly coordinating anion), the monometallic zinc complex **1** was reacted with one equivalent of the corresponding coinage metal salts [Au(tht)$_2$][SbF$_6$] (tht = tetrahydrothiophene), AgSbF$_6$ and [Cu(MeCN)$_4$][PF$_6$] (Scheme 2). This type of insertion of a coinage metal cation between the two phosphine units in the PNac scaffold is possible because the soft phosphine donors coordinate less preferentially to the hard zinc ion than the hard nitrogen donors. After filtration of the reaction mixture, single crystals of the respective compounds were obtained by slow evaporation for **2** and **3**, or by layering the THF solution with *n*-pentane for **4**. While the monometallic precursor **1** crystallizes in the monoclinic space

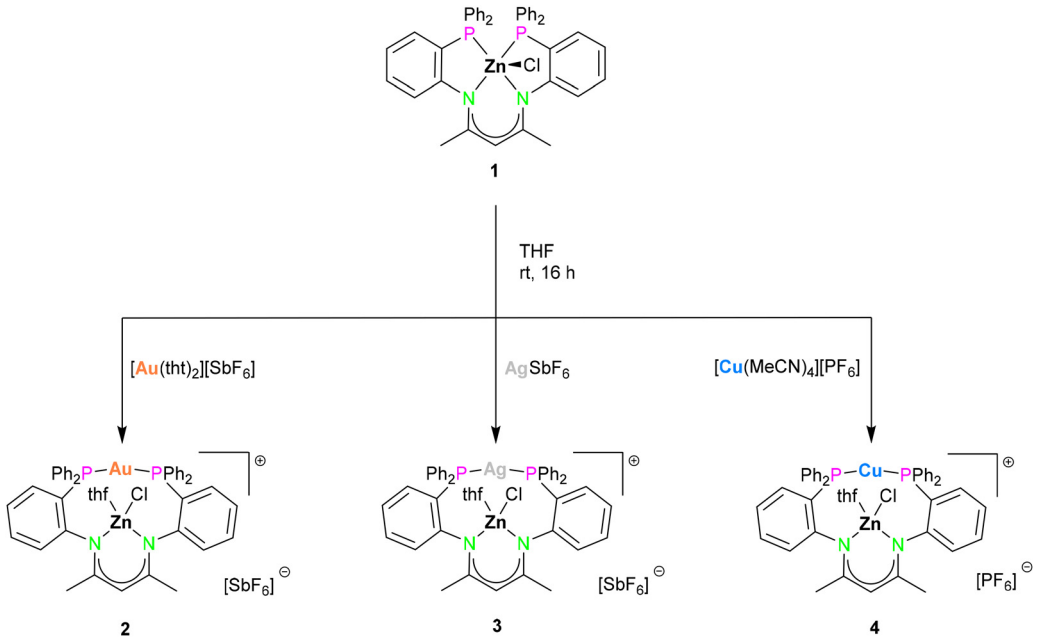

Scheme 2 Syntheses of ionic bimetallic compounds [PNacZnCl(thf)Au][SbF_6] (**2**), [PNacZnCl(thf)Ag][SbF_6] (**3**) and [PNacZnCl(thf)Cu][PF_6] (**4**).

group $P2_1/n$ with one molecule in the asymmetric unit, compounds **2–4** crystallize in the triclinic space group $P\bar{1}$ with one molecule in the asymmetric unit.

In the three isostructural bimetallic complexes (Fig. 4), the coinage metal ion is coordinated almost linearly by both phosphine units, whereby a definite trend of increasing linearity within the group 11 elements towards gold can be observed (**2**: 175.27(4)°; **3**: 167.95(8)°; **4**: 158.50(3)°). The central zinc metal is tetrahedrally coordinated by two N atoms of the PNac ligand, one chloride atom and one THF molecule. Therefore, the molecular structures are comparable to those of the neutral bimetallic complexes [$PNacMZnCl_2$] (M = Au, Ag),[32] except that the coordinating THF molecule replaces the chloride anion, which was in the *trans*-position to the coinage metal ion. The M···Zn distance in compounds **2–4** increases within group 11 from copper (2.7675(4) Å) *via* silver (2.9649(11) Å) to gold (2.9709(5) Å) as expected due to the increasing ionic radii. The large difference between the M···Zn distance of compounds **3** and **4** (0.1974 Å) could be attributed not only to the increase in ionic radius but also to a bridging effect of the

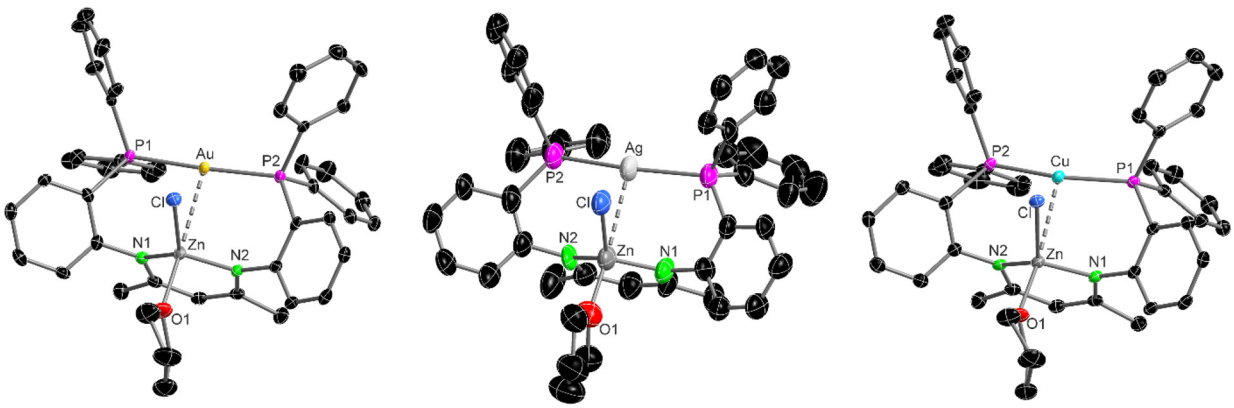

Fig. 4 Molecular structure of [PNacZnCl(thf)Au][SbF_6] (**2**) (left), [PNacZnCl(thf)Ag][SbF_6] (**3**) (center) and [PNacZnCl(thf)Cu][PF_6] (**4**) (right) in the solid state, with ellipsoids drawn at 50% probability. Hydrogen atoms, counterions and non-coordinating THF molecules are omitted for clarity. Selected distances [Å] and angles [°]: **2**: Au···Zn 2.9709(5), Au–P1 2.3073(9), Au–P2 2.3033(9), Zn–N1 1.959(3), Zn–N2 1.971(3), Zn–Cl 2.1812(9), Zn–O1 2.051(3); P1–Au–P2 175.27(4), N1–Zn–N2 96.38(12), Au–Zn–Cl 74.70(3), Au–Zn–O1 177.48(8), and O1–Zn–Cl 102.91(9). **3**: Ag···Zn 2.9649(11), Ag–P1 2.413(2), Ag–P2 2.412(2), Zn–N1 1.952(6), Zn–N2 1.972(7), Zn–Cl 2.209(2), Zn–O1 2.005(6); P1–Ag–P2 167.95(8), N1–Zn–N2 96.8(3), Ag–Zn–Cl 67.88(6), Ag–Zn–O1 172.6(2), and O1–Zn–Cl 104.9(2). **4**: Cu···Zn 2.7675(4), Cu–P1 2.2262(7), Cu–P2 2.2278(7), Cu···Cl 2.5245(7), Zn–N1 1.953(2), Zn–N2 1.949(2), Zn–Cl 2.2128(6), Zn–O1 2.001(2); P1–Cu–P2 158.50(3), N1–Zn–N2 97.35(8), Cu–Zn–Cl 59.68(2), Cu–Zn–O1 167.15(6), and O1–Zn–Cl 107.76(6).

chloride ion, as compound **4** displays the smallest M–Zn–Cl bond angle of 59.68°. In turn, the very small difference between the M···Zn distance in compounds **2** and **3** (0.006 Å) could be attributed to possible metallophilic interactions. Such interactions are not observed in the corresponding neutral complexes [PNacMZnCl$_2$] (M = Au, Ag), which exhibit a significantly larger difference in the M···Zn distance (0.1147 Å).[32]

The $^{31}P\{^1H\}$ NMR signals of the compounds **2–4** strongly differ in their respective chemical shifts and are low-field shifted compared to the Zn complex **1** (δ = −26.6 ppm). The phosphorus resonance of the phosphine donor units in compound **2** was detected at δ = 28.0 ppm, while in compound **3**, the phosphine signal was observed as two doublets at δ = −0.8 ppm (d, $^1J_{P,107Ag}$ = 519.2 Hz, $^1J_{P,109Ag}$ = 600.0 Hz), and is shifted to lower frequencies compared to that of **2**. The phosphine signal of compound **4** is further high-field shifted at δ = −7.4 ppm. The chemical shifts of compounds **2** and **3** are comparable to those of the corresponding neutral complexes [PNacMZnCl$_2$] (M = Au, Ag), which exhibit resonances at δ = 25.7 ppm and δ = −2.3 ppm, respectively.

In addition to the neutral group 11/group 12 complexes [PNacMZnCl$_2$],[32] a neutral gold–copper complex, [PNacAuCuI], is also known from the literature as the only reported example of a bimetallic species containing only group 11 metals featuring the PNac ligand.[32] Similar to the synthesis of complexes **2–4**, the corresponding ionic bimetallic complex [PNacAuCu(MeCN)][OTf] (**5**) was isolated by reacting equimolar amounts of the copper salt [Cu(MeCN)$_4$][OTf] with the literature-known monometallic gold complex [PNacAu] (Scheme 3). Suitable crystals for single-crystal X-ray diffraction analysis were grown by laying the filtered THF reaction mixture with *n*-pentane. Attempts to obtain other heterobimetallic coinage metal complexes, which are isostructural to **5**, from [PNacAu] or [PNacAg] were not successful.

Complex **5** crystallizes in the orthorhombic space group *Pnma* with two half-molecules in the asymmetric unit. The molecular structure of the non-disordered molecule is displayed in Fig. 5. The Au1···Cu1 distance of 2.7161(10) Å is about 0.08 Å longer than in the neutral complex [PNacAuCuI] with 2.634(2) Å.[32] The Au1–P1 (2.3121(14) Å) and Cu1–N1 (1.954(5) Å) bond lengths are almost identical compared to the neutral complex, while the P1–Au1–P1′ (172.48(8)°) and N1–Cu1–N1′ (96.1(3)°) bond angles are about 3° and 0.5° larger, respectively. The gold atom in complex **5** is slightly more linearly coordinated than in the ionic zinc complex **2**. In the

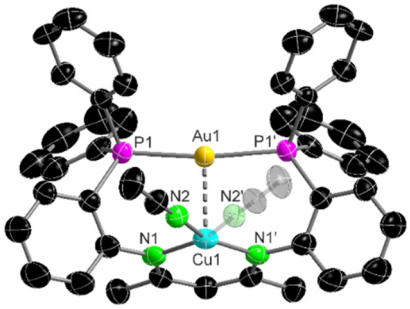

Fig. 5 Molecular structure of [PNacAuCu(MeCN)][OTf] (**5**) in the solid state, with ellipsoids drawn at 50% probability. The crystal structure shows certain disordered acetonitrile molecules. For reasons of clarity, hydrogen atoms, counterions and non-coordinating solvent molecules are not shown, but only the monomeric unit with the highest occupation probability. Selected distances [Å] and angles [°]: Au1···Cu1 2.7161(10), Au1–P1 2.3121(14), Cu1–N1 1.954(5), Cu1–N2 1.922(8), P1–Au1–P1′ 172.48(8), N1–Cu1–N1′ 96.1(3), Au1–Cu1–N2 99.6(3), N1–Cu1–N2 107.2(3), and N1′–Cu1–N2 156.7(3).

neutral complex [PNacAuCuI],[32] the copper ion in **5** exhibits a trigonal planar coordination geometry. However, instead of an iodide ion, an acetonitrile molecule occupies the free coordination site of the copper atom. The $^{31}P\{^1H\}$ NMR spectrum shows the phosphine signal of **5** at δ = 28.7 ppm, which is comparable to that of the bimetallic neutral complex [PNacAuCuI] (δ = 27.1 ppm) and the monometallic precursor [PNacAu] (δ = 28.6 ppm).

Photoluminescence properties

The bimetallic compounds **2–5** were investigated for their photoluminescent behavior in the solid state and in THF solution in order identify differences between the neutral complexes ([PNacMZnCl$_2$] (M = Ag, Au), [PNacAuCuI])[32,47] and the ionic complexes **2–4**. The monometallic precursor **1** was also studied in the solid state. This yellow solid exhibited cyan photoluminescence at both low temperature (77 K) and room temperature (298 K) (Fig. 6). The colorless to beige solids of complexes **2–4** and their THF solutions exhibited blue photoluminescence at both low temperature (77 K) and room temperature (298 K) (Fig. 7 and 8). Compound **5** is a yellow solid, which also forms yellow THF solutions. These displayed yellow

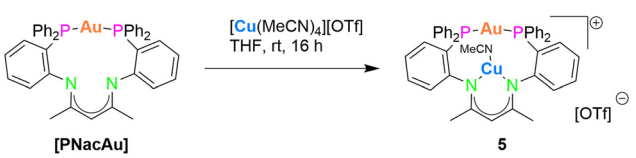

Scheme 3 Synthesis of the ionic bimetallic compound [PNacAuCu(MeCN)][OTf] (**5**).

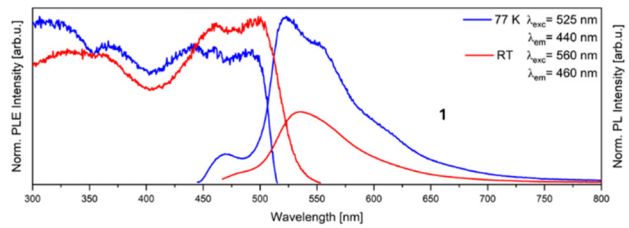

Fig. 6 Solid-state photoluminescence (PL) emission and excitation (PLE) spectra of monometallic complex **1** at 77 K (blue) and 298 K (red). PL and PLE spectra were recorded at the specified wavelengths (λ_{exc} and λ_{em}).

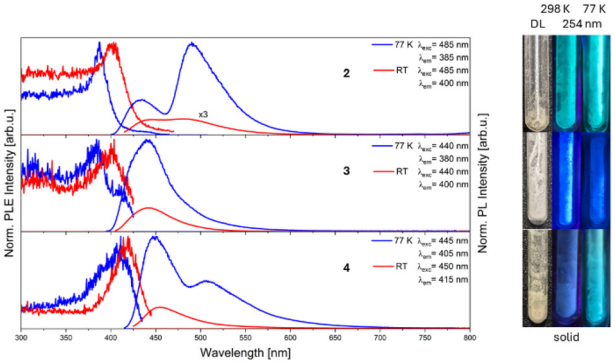

Fig. 7 Solid-state photoluminescence (PL) emission and excitation (PLE) spectra of Zn^{II} compounds **2–4** at 77 K (blue) and 298 K (red). PL and PLE spectra were recorded at the specified wavelengths (λ_{exc} and λ_{em}). Pictures of the compounds in daylight (DL) (left), under 254 nm UV light (middle) at 298 K, and under 254 nm UV light at 77 K (right).

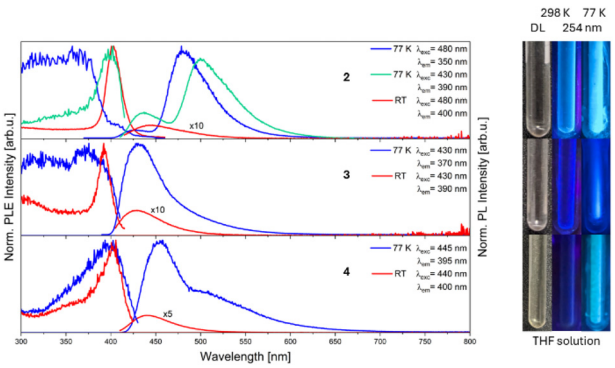

Fig. 8 Photoluminescence (PL) emission and excitation (PLE) spectra of Zn^{II} compounds **2–4** in THF solution at 77 K (blue/green) and 298 K (red). PL and PLE spectra were recorded at the specified wavelengths (λ_{exc} and λ_{em}). Pictures of the compounds in daylight (DL) (left), under 254 nm UV light (middle) at 298 K, and under 254 nm UV light at 77 K (right).

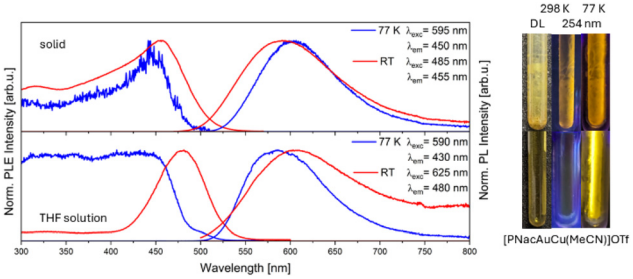

Fig. 9 Photoluminescence (PL) emission and excitation (PLE) spectra of **5** in the solid state (top) and in THF solution (bottom) at 77 K (blue) and 298 K (red). PL and PLE spectra were recorded at the specified wavelengths (λ_{exc} and λ_{em}). Pictures of the compounds in daylight (DL) (left), under 254 nm UV light (middle) at 298 K, and under 254 nm UV light at 77 K (right).

to orange photoluminescence at both low temperature (77 K) and room temperature (298 K) (Fig. 9).

The solid-state PL spectrum of the monometallic zinc compound **1** exhibits a low-intensity emission band at short wavelengths (470 nm) at low temperatures (77 K), followed by a broad emission band with a maximum at 525 nm and two shoulders at 550 nm and 595 nm. Compounds **2–4** display similar hypsochromic shifts in their emission bands compared to their precursor **1**, although their spectra differ significantly. At low temperature, the bimetallic zinc–gold complex **2** exhibits two emission maxima of different intensity at 435 nm and 490 nm. The long-wavelength emission maximum also lies in the same region as the single emission band (460–580 nm) of the neutral complex [PNacAuZnCl$_2$],[32] clearly showing the differences between the two species. For the zinc–silver complex **3**, a single emission maximum at 440 nm is observed at both low and room temperature. Furthermore, no additional bathochromic shoulder is detected in comparison to the neutral complex [PNacAgZnCl$_2$], which displays a shoulder at 490 nm.[32] At low temperature, the zinc–copper compound **4** exhibits two emission maxima at 445 nm and 505 nm, while the second maximum cannot be detected at room temperature. The photoluminescence excitation (PLE) spectra of compounds **2** and **3** at low temperature exhibit maxima at 385 nm. In addition, a shoulder around 410 nm is observed in the spectrum of **3**. The excitation maximum of **4** at low temperature is located at 410 nm, making it the least blue-shifted among compounds **2–4** compared to the monometallic precursor **1**, which shows a PLE onset at about 510 nm. The PL and PLE spectra of compound **2** frozen in THF solution display certain peculiarities compared to the PL and PLE spectra in the solid state. The intensity ratio of the two emission bands at 425 and 480 or 440 and 500 nm appears to depend on the excitation wavelength. At room temperature, this more intense long-wavelength maximum is no longer observed; only the shorter-wavelength maximum remains, slightly red-shifted to 445 nm. In contrast, only slight changes are observed in the PL spectra of compounds **3** and **4** in THF solution. The PL spectra of **3** remain hypsochromic, with maxima at 430 nm, shifted by 10 nm compared to the solid-state emission maxima at 440 nm, both at low and room temperature. The intense emission maximum of the PL spectrum of **4** at 460 nm is red-shifted by 10 nm in THF solution at low temperature, while this emission band undergoes a blue shift of 20 nm to 440 nm at room temperature. In turn, the weaker long-wavelength emission maximum loses intensity in solution at low temperature at 510 nm compared to the solid state.

Compared to the zinc–coinage metal complexes, the PL and PLE spectra of the bimetallic gold–copper complex **5** are shifted to the longer wavelength range. The emission bands and their maxima are clearly broadened at both low and room temperature, which can be observed both in the solid state and in the THF solution, similar to the precursor [PNacAu] and the neutral complex [PNacAuCuI], both with emission maxima at 620 nm at low temperature.[32] The emission maximum of **5** in the solid state at low temperature is observed at 605 nm and is blue-shifted by 15 nm at room temperature. In turn, a red shift from 585 nm to 605 nm can be observed in

Table 1 Experimentally determined data of the PLE and PL spectra as well as the lifetimes of compounds **2–5**

		$\lambda_{max,\ exc}$ [nm]		$\lambda_{max,\ em}$ [nm]		Φ_{PL} [%]	τ [μs]	
		77 K	298 K	77 K	298 K	298 K	77 K	298 K
1	Solid	440	460	470	485		—[a]	—[a]
[PNacZn]				525	535	75		
				550	560			
				595				
2	Solid	385	400	435	445		6	6
$[PNacZnAu]^+$				490	480	28	7/351	13
	Solved	355	405	425	445		—	6
				480			6/218/724	
		400		440			6	
				500			6/8/687	
3	Solid	385	400	440	440	41	6	6
$[PNacZnAg]^+$	Solved	370	390	430	430		6	6
4	Solid	410	420	450	455	6	6	6
$[PNacZnCu]^+$				505			6	
	Solved	395	405	450	440		6	6
5	Solid	445	455	605	590	55	40/103	7
$[PNacAuCu]^+$	Solved	430	480	585	605		62/163	7

[a] Below the limit value for phosphorescence lifetime determination.

solution during the transition from low to room temperature. In both states, the PLE spectra exhibit bathochromic shifts upon warming to room temperature. At room temperature in THF, there is a pronounced maximum at 480 nm, whereas at low temperature, no comparative maximum is seen, but rather a uniform band <450 nm. Compared to the neutral complex [PNacAuCuI], the bandwidth and the shift of the maxima are smaller, although the bands remain within the same wavelength range (520–730 nm).[32] The PL emissions of the ionic complexes **2–5** indicate luminescent processes with experimentally determined decay times of up to several hundred microseconds (Table 1). We identify these processes as phosphorescent, based on the significant decrease in intensity observed in the PL spectra at room temperature compared to low temperature. The kinetics of these processes involve several components, and the lifetimes τ had to be derived using up to three exponential fits. The longest lifetime of the excited state in both the solid state and THF solution was measured for zinc–gold complex **2**, corresponding to 351 μs in the solid state and 724 μs in solution. This lifetime extension in solution has otherwise only been measured for gold–copper complex **5**. In general, the decay times are temperature-dependent and decrease sharply at room temperature, as competing non-radiative relaxations are favored with increased temperatures. Because of the structural and spectral similarities, we assume that the quantum chemical calculation statements we previously published for the neutral complexes[32] can also be applied to the ionic complexes described here, with some reservations. Changes in luminescence due to the introduction of the second metal ion result from a cooperative effect between the two metal ions and the anionic $[NH–(CH)_3–NH]^-$ fragment. For complex **5**, the metallophilic interaction between Au(I) and Cu(I) is also likely to have an additional influence. Based on this, it is likely that there are no metallophilic interactions for complexes **2–4**.[32]

Conclusions

We presented a synthetic protocol for the preparation of a series of cationic heterobimetallic complexes featuring the PNac scaffold as an orthogonal ligand. The molecular structures of the resulting complexes differ from the neutral complexes known from the literature by the absence of one coordinated halide ion, which is replaced by a solvent molecule at the vacant coordination site. In addition to these structural changes in the complexes, we found that the PL properties also differ between the neutral and the respective cationic complexes. In general, as previously observed for the neutral complexes, the presence of two different metals within the same ligand backbone exerts a significant influence on the photoluminescence properties. The zinc–coinage metal complexes **2–4** exhibited blue emission in the wavelength range of 400–550 nm. In contrast, the gold–copper complex **5** showed yellow- to orange-colored emissions in the range of 525–700 nm. We were able to experimentally determine decay times for phosphorescent processes of up to several hundred microseconds.

Conflicts of interest

There are no conflicts to declare.

Data availability

The following data are part of the SI: synthesis and characterization, NMR spectra, IR spectra, Raman spectra, photoluminescence data, and X-ray crystallography. NMR, IR, EA and PL data supporting the findings of this study are available on Radar4Chem under the identifier **https://doi.org/10.22000/**

9tz9nn9r57bmh7sd. See DOI: https://doi.org/10.1039/d5dt00977d.

CCDC 2446444–2446448 contain the supplementary crystallographic data for this paper.[56a–e]

Acknowledgements

The authors acknowledge support from the Deutsche Forschungsgemeinschaft through grant no. 540378534, RO 2008/22-1. We would like to thank Dr. Christian Ritschel and Prof. Dr. Claus Feldmann for their support with measuring the quantum yield.

References

1 V. Balzani, A. Juris, M. Venturi, S. Campagna and S. Serroni, *Chem. Rev.*, 1996, **96**, 759–834.
2 V. W.-W. Yam, K. K.-W. Lo and K. M.-C. Wong, *J. Organomet. Chem.*, 1999, **578**, 3–30.
3 V. W.-W. Yam and K. K.-W. Lo, *Chem. Soc. Rev.*, 1999, **28**, 323–334.
4 C.-M. Che and S.-W. Lai, *Coord. Chem. Rev.*, 2005, **249**, 1296–1309.
5 C. Yue, C. Yan, R. Feng, M. Wu, L. Chen, F. Jiang and M. Hong, *Inorg. Chem.*, 2009, **48**, 2873–2879.
6 C. Uhlmann, T. J. Feuerstein, T. P. Seifert, A. P. Jung, M. T. Gamer, R. Köppe, S. Lebedkin, M. M. Kappes and P. W. Roesky, *Dalton Trans.*, 2022, **51**, 10357–10360.
7 M. K. Rong, F. Holtrop, J. C. Slootweg and K. Lammertsma, *Coord. Chem. Rev.*, 2019, **382**, 57–68.
8 J. A. Mata, F. E. Hahn and E. Peris, *Chem. Sci.*, 2014, **5**, 1723–1732.
9 R. Maity, B. S. Birenheide, F. Breher and B. Sarkar, *ChemCatChem*, 2021, **13**, 2337–2370.
10 S. Patra and N. Maity, *Coord. Chem. Rev.*, 2021, **434**, 213803.
11 S. Liu, A. Motta, A. R. Mouat, M. Delferro and T. J. Marks, *J. Am. Chem. Soc.*, 2014, **136**, 10460–10469.
12 M. Navarro, J. J. Moreno, M. Pérez-Jiménez and J. Campos, *Chem. Commun.*, 2022, **58**, 11220–11235.
13 J. Serrano-Plana, I. Garcia-Bosch, A. Company and M. Costas, *Acc. Chem. Res.*, 2015, **48**, 2397–2406.
14 E. Mas-Marzá, J. A. Mata and E. Peris, *Angew. Chem., Int. Ed.*, 2007, **46**, 3729–3731.
15 A. Zanardi, J. A. Mata and E. Peris, *J. Am. Chem. Soc.*, 2009, **131**, 14531–14537.
16 A. Zanardi, R. Corberán, J. A. Mata and E. Peris, *Organometallics*, 2008, **27**, 3570–3576.
17 A. Zanardi, J. A. Mata and E. Peris, *Organometallics*, 2009, **28**, 4335–4339.
18 M. Böhmer, G. Guisado-Barrios, F. Kampert, F. Roelfes, T. T. Y. Tan, E. Peris and F. E. Hahn, *Organometallics*, 2019, **38**, 2120–2131.
19 M. Böhmer, F. Kampert, T. T. Y. Tan, G. Guisado-Barrios, E. Peris and F. E. Hahn, *Organometallics*, 2018, **37**, 4092–4099.
20 V. W.-W. Yam and E. C.-C. Cheng, *Photochemistry and Photophysics of Coordination Compounds II*, Springer, Berlin, Heidelberg, 2007.
21 M. J. Calhorda, C. Ceamanos, O. Crespo, M. C. Gimeno, A. Laguna, C. Larraz, P. D. Vaz and M. D. Villacampa, *Inorg. Chem.*, 2010, **49**, 8255–8269.
22 H. Schmidbaur and A. Schier, *Angew. Chem., Int. Ed.*, 2015, **54**, 746–784.
23 R. L. White-Morris, M. M. Olmstead and A. L. Balch, *J. Am. Chem. Soc.*, 2003, **125**, 1033–1040.
24 M. Sarkar, *Inorg. Chim. Acta*, 2024, **572**, 122275.
25 K. Uemura and R. Miyake, *Inorg. Chem.*, 2020, **59**, 1692–1701.
26 P. Pyykkö, *Chem. Rev.*, 1997, **97**, 597–636.
27 A. Ceccon, S. Santi, L. Orian and A. Bisello, *Coord. Chem. Rev.*, 2004, **248**, 683–724.
28 P. Aguirre-Etcheverry and D. O'Hare, *Chem. Rev.*, 2010, **110**, 4839–4864.
29 S. Bestgen, M. T. Gamer, S. Lebedkin, M. M. Kappes and P. W. Roesky, *Chem. – Eur. J.*, 2015, **21**, 601–614.
30 M. Dahlen, E. H. Hollesen, M. Kehry, M. T. Gamer, S. Lebedkin, D. Schooss, M. M. Kappes, W. Klopper and P. W. Roesky, *Angew. Chem., Int. Ed.*, 2021, **60**, 23365–23372.
31 M. Dahlen, M. Kehry, S. Lebedkin, M. M. Kappes, W. Klopper and P. W. Roesky, *Dalton Trans.*, 2021, **50**, 13412–13420.
32 F. Krätschmer, X. Sun, D. Frick, C. Zovko, W. Klopper and P. W. Roesky, *Inorg. Chem. Front.*, 2024, **11**, 853–862.
33 I. O. Koshevoy, Y.-C. Chang, A. J. Karttunen, M. Haukka, T. Pakkanen and P.-T. Chou, *J. Am. Chem. Soc.*, 2012, **134**, 6564–6567.
34 V. W.-W. Yam, V. K.-M. Au and S. Y.-L. Leung, *Chem. Rev.*, 2015, **115**, 7589–7728.
35 V. R. Naina, F. Krätschmer and P. W. Roesky, *Chem. Commun.*, 2022, **58**, 5332–5346.
36 R. G. Pearson, *J. Chem. Educ.*, 1968, 581–587.
37 R. G. Pearson, *J. Chem. Educ.*, 1968, 643–648.
38 R. G. Pearson, *Inorg. Chim. Acta*, 1995, **240**, 93–98.
39 T. Simler, K. Möbius, K. Müller, T. J. Feuerstein, M. T. Gamer, S. Lebedkin, M. M. Kappes and P. W. Roesky, *Organometallics*, 2019, **38**, 3649–3661.
40 T. P. Seifert, S. Bestgen, T. J. Feuerstein, S. Lebedkin, F. Krämer, C. Fengler, M. T. Gamer, M. M. Kappes and P. W. Roesky, *Dalton Trans.*, 2019, **48**, 15427–15434.
41 Shubham, V. R. Naina and P. W. Roesky, *Chem. – Eur. J.*, 2024, **30**, e202401696.
42 F. Völcker, F. M. Mück, K. D. Vogiatzis, K. Fink and P. W. Roesky, *Chem. Commun.*, 2015, **51**, 11761–11764.
43 C. Zovko, S. Bestgen, C. Schoo, A. Görner, J. M. Goicoechea and P. W. Roesky, *Chem. – Eur. J.*, 2020, **26**, 13191–13202.

44 S. Bestgen, M. Mehta, T. C. Johnstone, P. W. Roesky and J. M. Goicoechea, *Chem. – Eur. J.*, 2020, **26**, 9024–9031.
45 C. Zovko, F. Krätschmer, S. Schmidt, T. P. Seifert, M. T. Gamer and P. W. Roesky, *ChemPlusChem*, 2022, **87**, e202200288.
46 C. Zovko, *Synthese und Charakterisierung unterschiedlicher N,P-Ligandensysteme und deren Metallkomplexe sowie die Untersuchung ihrer photophysikalischen Eigenschaften*, Cuvellier Verlag, 2022.
47 F. Krätschmer, *Synthese von multinuklearen mono- und bimetallischen Verbindungen der Münzmetalle sowie die Untersuchung von Metall-Metall Wechselwirkung auf photophysikalische Eigenschaften*, Cuvellier Verlag, 2023.
48 A. Pinto, N. Svahn, J. C. Lima and L. Rodríguez, *Dalton Trans.*, 2017, **46**, 11125–11139.
49 C. Cunha, A. Pinto, A. Galvão, L. Rodríguez and J. S. Seixas De Melo, *Inorg. Chem.*, 2022, **61**, 6964–6976.
50 P. Alam, C. Climent, P. Alemany and I. R. Laskar, *J. Photochem. Photobiol., C*, 2019, **41**, 100317.
51 Z. Luo, X. Yuan, Y. Yu, Q. Zhang, D. T. Leong, J. Y. Lee and J. Xie, *J. Am. Chem. Soc.*, 2012, **134**, 16662–16670.
52 T. P. Seifert, V. R. Naina, T. J. Feuerstein, N. D. Knöfel and P. W. Roesky, *Nanoscale*, 2020, **12**, 20065–20088.
53 D. Rios, D. M. Pham, J. C. Fettinger, M. M. Olmstead and A. L. Balch, *Inorg. Chem.*, 2008, **47**, 3442–3451.
54 L. M. C. Luong, M. A. Malwitz, V. Moshayedi, M. M. Olmstead and A. L. Balch, *J. Am. Chem. Soc.*, 2020, **142**, 5689–5701.
55 A. L. Balch, *Angew. Chem., Int. Ed.*, 2009, **48**, 2641–2644.
56 (*a*) S. Kebernik, F. Krätschmer, X. Sun and P. W. Roesky, CCDC 2446444: Experimental Crystal Structure Determination, 2025, DOI: **10.5517/ccdc.csd.cc2n3qk2**; (*b*) S. Kebernik, F. Krätschmer, X. Sun and P. W. Roesky, CCDC 2446445: Experimental Crystal Structure Determination, 2025, DOI: **10.5517/ccdc.csd.cc2n3ql3**; (*c*) S. Kebernik, F. Krätschmer, X. Sun and P. W. Roesky, CCDC 2446446: Experimental Crystal Structure Determination, 2025, DOI: **10.5517/ccdc.csd.cc2n3qm4**; (*d*) S. Kebernik, F. Krätschmer, X. Sun and P. W. Roesky, CCDC 2446447: Experimental Crystal Structure Determination, 2025, DOI: **10.5517/ccdc.csd.cc2n3qn5**; (*e*) S. Kebernik, F. Krätschmer, X. Sun and P. W. Roesky, CCDC 2446448: Experimental Crystal Structure Determination, 2025, DOI: **10.5517/ccdc.csd.cc2n3qp6**.